



WGM: Wavelet-Based Gamma Model for Video Traffic in Wireless Multi-hop Networks

Hang Shen^{1,2} · Guangwei Bai¹ · Junyuan Wang¹ · Lu Zhao¹

Published online: 30 March 2019
© Springer Science+Business Media, LLC, part of Springer Nature 2019

Abstract

While most of the existing literature concentrates on wireless traffic characterization and its effects on network performance, relatively little research work has focused on mathematical modeling and queuing analysis of video traffic in wireless multi-hop networks. The purpose of this paper is to characterize and model wireless multi-hop network video traffic. We begin with thorough analysis and investigations of characteristics of video traffic in typical wireless network scenarios, building upon which we present a novel Wavelet-based Gamma Model (WGM) for wireless multi-hop video streaming. Our analytic and simulation results demonstrate that the WGM provides a flexible and robust means to characterize wireless video traffic, in terms of statistical properties and self-similarity. On this basis, a WGM queuing system is constructed to deduce the theoretical value of buffer overflow probability, delay and delay jitter for wireless media streaming. A series of simulation experiments are conducted to demonstrate the generality and effectiveness of our modeling approach. Our experimental results show that the probability of buffer overflow indicates a hyperbolic decay as the buffer size increases; however, the buffer overflow probability decays exponentially fast, as the sending rate increases. The study also finds that, as the buffer size increases, the delay and delay jitter of video streaming first increase then become stable, but with an increase in the sending rate, both values decrease sharply. We believe that this conclusion could contribute to the design of appropriate network architectures and to elaborate efficient wireless multimedia communication protocols.

Keywords Video traffic modeling · Self-similarity · Wireless multi-hop networks · Gamma distribution · Wavelet

✉ Guangwei Bai
bai@njtech.edu.cn

¹ Department of Computer Science and Technology, Nanjing Tech University, No. 30, PuZhu Road (South), Pukou District, Nanjing 211816, Jiangsu Province, China

² National Engineering Research Center of Communications and Networking (Nanjing University of Posts and Telecommunications), Nanjing 210003, China

1 Introduction

In recent years, the popularity of inexpensive video-enabled smartphones and high-speed wireless networks has facilitated the introduction of emerging mobile multimedia applications. An *Ericsson Mobility Report* [1] released in 2017 indicates that wireless video traffic is expected to grow by about 50% by 2022, becoming nearly 75% of all mobile data traffic. However, characteristics such as user mobility, dynamic channel and topology changes, high error rate, and limited bandwidth of wireless networks, coupled with diversification, high rate, and high bursty of multimedia communication, can render network traffic extremely complicated. A method to construct an accurate multimedia traffic model, to facilitate effective and efficient network parameters estimation, to provide adequate Quality-of-Service (QoS) to users is a very challenging problem.

Traffic analysis and modeling are the basis of network performance monitoring and management, protocol design and QoS provisioning, which is of great significance to the planning and design of wireless multimedia services. Previous studies have confirmed that the traffic in high-speed networks has apparent self-similar nature [2], which manifests as long-range dependence (LRD) and heavy-tailed distribution with infinite variance. Due to the self-similar property of traffic, there is more occupation of buffer and larger delay than the results predicted by traditional queuing analysis, which results in significant performance degradation (such as high packet loss [3], traffic congestion [4], unbounded network latency [5] and degraded network stability [6]). It is feasible to provide scientific theoretical support for performance evaluation and protocol design by studying self-similar features and finding models that can characterize and predict self-similar traffic (including frame size [7, 8], packet loss rate [9], queue length [10], and so on). However, the dynamic characteristics of wireless networks, coupled with the complexity of mixed network traffic, makes it difficult to model wireless streaming media accurately. Many of the early proposed traffic models (e.g., AFRP [11, 12], EAFRP [13], FBM [14], FARIMA [15], and wavelet model [16]) cannot accurately describe the characteristics of wireless traffic. While researchers have proposed many wireless traffic models [17–19], there are few studies on the self-similarity model and queuing analysis for video traffic in wireless multi-hop networks.

This work analyzes and models the video traffic in wireless multi-hop networks. To begin with, building upon the Wavelet Independent Gaussian (WIG) [16, 20] model and considering the inherent characteristics of a dynamic network environment and real-time video communication, a novel Wavelet-based Gamma Model (WGM) is proposed to more accurately describe the various characteristics of wireless video traffic. The WGM uses the Haar wavelet multi-resolution analysis to divide the time series into scale space and wavelet space, then models it in scale space and wavelet space respectively, and so produces model data of wireless streaming media by wavelet transform. Because scale coefficients approximately follow Gamma distribution, we use Gamma first-order autoregression model to produce the scale coefficients in the last scale space. In the wavelet space, we still use the WIG to provide wavelet coefficients. Through an in-depth analysis of probability statistics and autocorrelation of simulation data and model data, we find that the WGM can describe streaming media in two different wireless scenarios well. Finally, we build the WGM queuing system to deduce the theoretical value of buffer overflow probability, delay and delay jitter of wireless media streaming concerning with respect to buffer size and sending rate, and we conduct simulations to characterize the performance of wireless multi-hop video streaming further.

The remainder of this paper is organized as follows. We briefly introduce the related works and our motivation in the next section. In Sect. 3, a Wavelet-based Gamma Model is proposed from an in-depth analysis of wireless video traffic. The accuracy of our model is analyzed and evaluated in Sect. 4, followed by a queuing system that quantifies overflow probability, delay, and delay jitter of wireless video streaming in Sect. 5. Finally, based on simulation data and model data, the buffer overflow probability, delay and delay jitter of wireless video streaming are simulated numerically, and the characteristics with the change of buffer size and sending rate are obtained in Sect. 6 before concluding in Sect. 7.

2 Background and Related Works

2.1 Self-Similarity of Network Traffic

The self-similarity phenomenon of network traffic has been reasonably well studied in the literature. Leland et al. [21] demonstrated that Ethernet communication is abrupt across multiple time scales and can be described as statistically self-similar (1994). This research poses a challenge to the Poisson assumptions in traditional network traffic models, indicating that the study on network traffic model has stepped into a new stage. Since then, Crovella and Bestavros [22] reported that Web traffic has self-similarity. Our research [23] showed that the self-similarity of web traffic does not change with the introduction of proxy. Studies have found that self-similarity also exists in multimedia traffic [24]. By analyzing the backbone link traffic of Tier 1 ISP, Karagiannis et al. [25] found that the high bandwidth and high aggregate link traffic approximates the Poisson process at small scale, which raises controversy over network traffic model, but this does not mean traffic does not have self-similar nature. Borgnat et al. [26] analyzed the traffic of the trunk link across the Pacific for seven years and found that LRD remains robust, sustained and stable, and the trend that the edge distribution of the aggregated traffic evolves towards Gaussian distribution tends to be stable over time. All of these studies have revealed that the high-speed network traffic has self-similarity features statistically; regardless of network topology, the number of users, types of services and applications, self-similarity always exists.

2.2 Wireless Traffic Analysis

Many researchers explore the statistical characteristics of traffic in various wireless networks. The study in [27] showed that wireless ad-hoc network traffic exhibits self-similar characteristics with LRD. Tickoo et al. [28] developed an analytic model to characterize the interarrival time distribution of traffic in wireless ad-hoc networks. Simulation results show that a separate video stream is self-similar, while the aggregation traffic has multi-fractal characteristics. The experimental results in [29] demonstrate that the self-similarity of aggregation traffic in WLANs becomes more marked as network load increases; the smaller the sampling interval, the more self-similarity there is; the self-similarity of TCP traffic is higher than that of UDP traffic. Petropulu et al. [30] explored the case when wired traffic is passed to a wireless network through a gateway, found that when the gateway works in the power control mode and its buffer area is much larger than the capacity of the wireless channel capacity, the self-similarity can decrease and even disappear.

2.3 Wireless Traffic Modelling

Only a small amount of literature is related to the study of wireless self-similar traffic models. Ge et al. [31] proposed a frame traffic model by analyzing the influence of different frame types on the self-similarity of the aggregated frame service in 802.1 WLANs. The purpose is to change the self-similarity of the aggregated frame traffic by adjusting the average frame size and the ratio of specified frame types, thereby improving channel utilization and throughput. Kastrinakis et al. [8] proposed a video traffic model with Markov chains and the Jaccard index similarity coefficient as an H.264 video traffic generator over wireless networks. Li et al. [32] presented an analytical model for wireless multimedia traffic, involving the fractional Brownian motion to simulate the self-similar traffic behavior. A spatial correlation and mobility-aware traffic model for wireless sensor networks was presented in [17] for wireless sensor networks. The model predicts that the aggregated traffic exhibits the bursty feature characterized by a scaled power-law decayed autocovariance function.

The video service has become the main traffic in mobile Internet, but the existing literature lacks the research on the video traffic model of wireless multi-hop networks, which drives us to construct an accurate traffic model and carry out a queuing analysis.

3 Wavelet-Based Gamma Model (WGM)

Many studies on network traffic characteristics show that network traffic in real environments presents a relatively significant scaling feature. The wavelet transform has a natural ability for scale analysis, suitable for describing network traffic. In this work, model data generation process is as follows: first, the Haar wavelet transform is used to analyze the data series generated by an experiment, and thus the scale space and wavelet space of the data series are obtained. Then, the data are modeled in the scale space and the wavelet space, respectively. Finally, the model data is obtained using the inverse wavelet transform.

3.1 Scale Space Modeling

Two experiments scenarios are constructed to collect traffic data samples. Nodes cannot move in Scenario I (say *static multi-hop network*) and can move in Scenario II (say *dynamic multi-hop network*). For the former, we build an 802.11 wireless network with three hops, where there is only one MPEG video connection, and no background communication exists. For the latter, we set up an 802.11 wireless network that has a random distribution of many nodes in moving status, where there is an MPEG video session and multiple different types of cross sessions (non-video) as background traffic. After capturing video traffic data transmitted at the network layer, we acquire the amount of data transferred per second.

The experimental data collected is decomposed into the third grade with Haar wavelet multi-resolution to obtain the “smallest” scaling coefficients. The empirical probability of the scaling coefficient is calculated and fitted by Gaussian distribution and Gamma distribution, respectively.

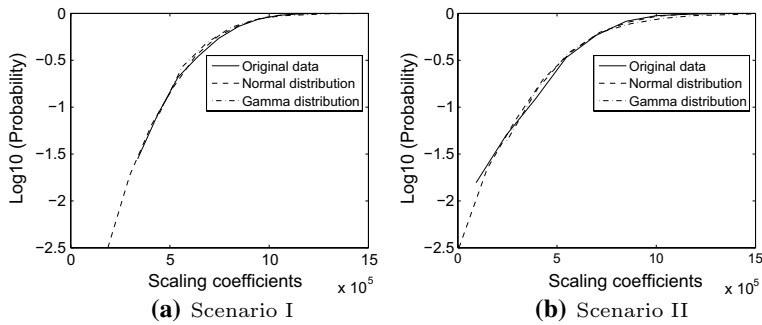


Fig. 1 Probability of scaling coefficients

As shown in Fig. 1, Gamma distribution can fit the probability properties of the scaling coefficient well, while the data generated by Gaussian distribution shows expansion in numerical range and cannot fit the scaling coefficient well. We use the Gamma first-order autoregression model (referred to as GAR(1)) to simulate the scaling coefficients.

Definition 1 (GAR(1)) In general, suppose X_k is a stationary series. If

$$X_k = \rho \cdot X_{k-1} + \varepsilon_k, \quad 0 < \rho < 1 \quad (1)$$

in which $\{\varepsilon_k\}$ is a random series independent of X_k and follows the Gamma edge distribution, then $\{X_k\}$ is the data series satisfying GAR(1).

The general formula for the probability density of Gamma distribution is

$$f(x) = \frac{1}{\Gamma(a)} \cdot \lambda^a \cdot x^{a-1} \cdot e^{-\lambda x}, \quad x \geq 0; a, \lambda > 0 \quad (2)$$

where α is shape parameter, λ is scale parameter, and $\Gamma(\cdot)$ represents Gamma function

$$\Gamma(a) = \int_0^\infty \mu^{a-1} \cdot e^{-\mu} \cdot d\mu \quad (3)$$

It can be seen that GAR(1) has three parameters ρ, α, λ . They need to be estimated from real traffic data in order to fit the real video traffic source.

The mean and variance of $\{\varepsilon_k\}$ are expressed as

$$\mathbb{E}(\varepsilon) = \frac{a}{\lambda}, \quad \mathbb{D}(\varepsilon) = \frac{a}{\lambda^2} \quad (4)$$

Suppose

$$\mathbb{E}(X) = m, \quad \mathbb{D}(X) = v \quad (5)$$

then

$$\begin{cases} \mathbb{E}(\varepsilon) = (1 - \rho) \cdot \mathbb{E}(X) = (1 - \rho) \cdot m \\ \mathbb{D}(\varepsilon) = (1 - \rho^2) \cdot \mathbb{D}(X) = (1 - \rho^2) \cdot v \end{cases} \quad (6)$$

From (4) and (6), α and λ can be deduced as

$$\alpha = \frac{(1 - \rho) \cdot m^2}{(1 - \rho) \cdot v}, \quad \lambda = \frac{m}{(1 - \rho) \cdot v} \quad (7)$$

Based on Eq. (1), we can estimate ρ through least squares method.

$$\hat{\rho} = \frac{\sum_{i=2}^N (X_i - m) \cdot (X_{i-1} - m)}{\sum_{i=2}^N (X_{i-1} - m)^2} \quad (8)$$

3.2 Wavelet Space Modeling

The modeling of wavelet coefficients for video streaming is carried out in both probability distribution and self-similarity. It is well known that wavelet transform has an excellent whitening effect on self-similar signals, and the wavelet coefficients are almost irrelevant in the wavelet domain. Following the lemma derived from [33] well describes the whitening effect of the Haar wavelet.

Lemma 1 Let $x(t)$ be a self-similar fractal Gaussian noise (FGN) signal whose Hurst parameter is H ($0.5 < H < 1$) and $W_{j,k}$ is the Haar wavelet coefficient of $x(t)$. The correlation coefficient of $W_{j,k}$ satisfies

$$E(W_{j_1,k_1}, W_{j_2,k_2}) \sim O(|2^{j_1} \cdot k_1 - 2^{j_2} \cdot k_2|^{-2H}) \quad (9)$$

Remark 1 From Lemma 1, the correlation coefficient decays very quickly as the scaling parameters j and the change in displacement parameter k . For the sake of simplicity, we assume that the wavelet coefficients at different levels and those that reach the same level at different times are irrelevant and can be modeled using irrelevant models.

The wavelet coefficients will be Gaussian distributed when $x(t)$ is a strict FGN signal, but the real video stream is usually not a strict FGN signal. Thus, a random variable probability distribution correction method is introduced.

Assume that the probability distribution function of the random variable x is $F_x(x)$. To obtain a set of random variables with the probability distribution $F_y(y)$, we can perform the following transformation

$$y = F_y^{-1}(F_x(x)) \quad (10)$$

By applying (10) to the process of wavelet coefficient modeling, we have

$$W_{j,k} = F_j^{-1}(N_j(x_{j,k})) \quad (11)$$

In Eq. (11), F_j^{-1} is the inverse of the empirical probability distribution function of the j -th wavelet coefficients; N_j is the Gaussian distribution function $N(\mu_j, \sigma_j)$, where μ_j and σ_j are the mean and standard deviation of the j -th-order wavelet coefficients; $x_{j,k}$ is the random variable that follows the distribution of $N(\mu_j, \sigma_j)$. In this way, we can find the wavelet coefficients at all levels of the model.

3.3 Data Synthesis

The model data of scale space and wavelet space can be generated using the model introduced above. The detailed process is as follows:

1. Determine the level number n of wavelet multi-resolution analysis, wavelet analysis of the real data, decompose to level n ; obtain one scale space (level 0) and n coefficients of wavelet space (from level 0 to level $n-1$);
2. Calculate the parameters of GAR model using scaling coefficients of real data and then use the model in Sect. 3.1 to generate the scaling coefficient $U_{0,k}$;
3. Estimate the mean and standard deviation of the wavelet coefficients at all levels to produce a Gaussian distribution series and to correct wavelet coefficients $W_{j,k}$ at all levels via the formula $W_{j,k} = F_{j-1}(N_j(x_j, k))$;
4. Using wavelet transform to obtain a simulated video stream, i.e.,

$$\widehat{G(t)} = \sum_{k=0}^{2^n-1} U_{0,k} \cdot \varphi_{0,k}(t) + \sum_{j=0}^n \sum_{k=0}^{2^j-1} W_{j,k} \cdot \psi_{j,k}(t) \quad (12)$$

4 Verification and Validation of the WGM

Based on the model presented in Sect. 3 and the experimental data generated, two different model data are generated for Scenarios I and II, respectively using the Matlab tool. The level of wavelet multi-resolution analysis is fixed to 3. In the following context, we first verify the self-similarity of model data, followed by a performance validation of the WGM.

4.1 Model Verification

We analyze self-similarity of data series generated by the WGM, involving the self-similarity coefficient, the variance–time (V–T) diagram, and the rescaled adjusted range (R/S) plot, according to the standard statistical analysis method in [21].

Figures 2 and 3 provide the autocorrelation properties of model data generated by the WGM, where the parameters of Gamma model are calculated using the experimental data generated with the method in Sect. 3 under Scenarios I and II.

The time series from Scenario I generated by the model is examined in Fig. 2a, where the model data has visible burstiness. From Fig. 2b, we can see that the autocorrelation function for the time series exhibits a hyperbolic attenuation trend, which is indicative of self-similarity. Figure 2c is the V–T graph for the time series, where the slope of the variance logarithm is greater than -1 . There is a slowly decaying variance for the aggregated time series, which is another indication of self-similarity. Figure 2d provides the R/S plot of the series, from which the self-similar parameter H of the model time series is estimated as 0.8094, confirming once again the existence of self-similarity. Similarly, as shown in Fig. 3, the data from Scenario I generated by the model also has visible self-similarity, and the Hurst parameter H can be estimated using the R/S method to be 0.8096.

4.2 Performance Validation

The results in Sect. 4.1 indicate that the model data generated by the WGM has prominent self-similar features. To further verify and evaluate its performance, a natural step is to compare it with the video stream data series produced by experiments.

Figures 4 and 5 give a comparison of the autocorrelation function, PDF (probability density function) and CDF (cumulative distribution function) curves of experimental

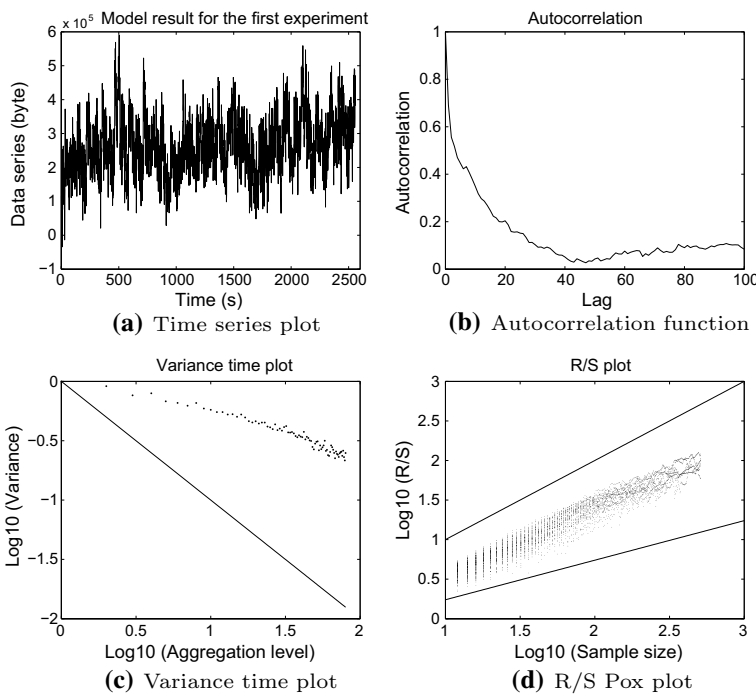


Fig. 2 Evidence of self-similarity of video traffic in Scenario I (model data)

data with model data for Scenarios I and II, respectively. The WGM fits statistical properties and autocorrelation characteristics of experimental data series well, indicating that it can accurately reflect the main characteristics of actual video traffic.

Figure 5a shows that the autocorrelation curve of model data is generally lower than that of experimental data. The gap between the two curves in the [60, 90] interval increases, but when Lag is 90, both tend to approach each other. This feature shows that the model reduces the autocorrelation of experimental data to a certain extent. The main reason for this is that the randomness of the model and the high packet loss rate of the dynamic network data are irregular. We can see Fig. 5b that the probability density curves of experimental data and model data are obviously different when the sample size of the time series is close to zero, but are very similar in the other regions. Careful analysis shows that the jump of experimental data series is caused by high packet loss rate when the sample value is close to 0. Turning to Fig. 5c, model data and experimental data are also slightly different in the vicinity of zero, which, however, the deviation gradually disappears as the value of data becomes more massive.

In Table 1, the self-similarity of the two data series is demonstrated by the Hurst parameter, and the effect of this slight deviation on the self-similarity of real-time video traffic can also be explained. The self-similarity of model data and experimental data are very similar, which further validates the accuracy of our model proposed in this paper. Moreover, we can see that the variation of the Hurst parameter of Scenario I is more significant than that of Scenario II by comparing the difference of self-similarity between simulated traffic and model traffic. This feature also confirms the deviation phenomenon observed in Fig. 5 in another way.

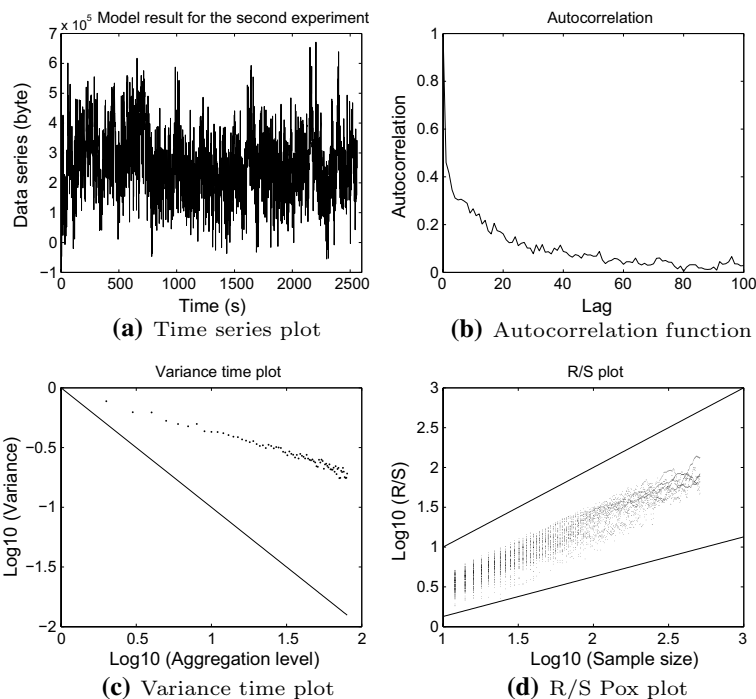


Fig. 3 Evidence of self-similarity of video traffic in Scenario II (model data)

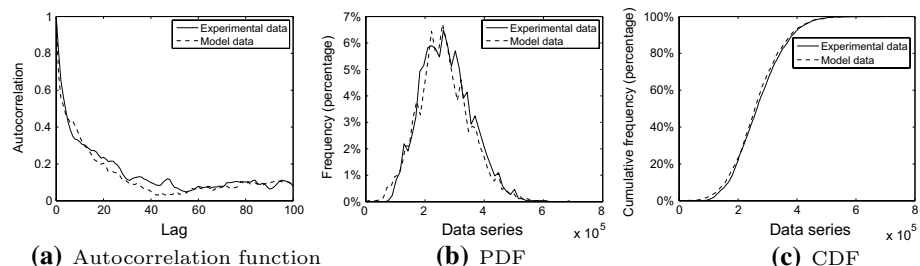


Fig. 4 Fitting degree between experimental data and model data for Scenario I

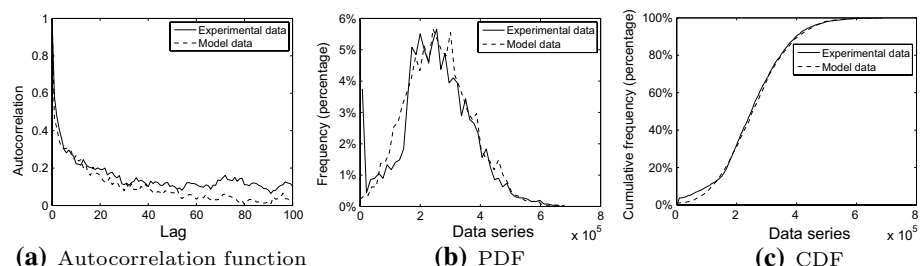


Fig. 5 Fitting degree between experimental data and model data for Scenario II

Table 1 Comparison of Hurst parameter

Scenario	Experimental data	Model data	Difference
I	0.8080	0.8094	- 0.0014
II	0.8184	0.8096	0.0088

5 WGM Queuing System

In the previous section, the accuracy of the WGM is verified, and thus it can be used as source traffic generators to evaluate video transmission performance over a wireless multi-hop network. In this section, the theoretical analysis of buffer overflow probability with the WGM under the framework of multi-scale queuing analysis is conducted, to provide a reference for the design of effective communication protocols and access control mechanisms.

5.1 Analysis of Multi-scale Queuing

Assuming that there is an unlimited first-in first-out (FIFO) buffer, the outflow probability is constant to C . Let Q_t denote the buffer length at time t , and $G(i)$ denote the traffic flow into the buffer, we have

$$Q_t = \sup_{s \geq 1} (G^{(s)} - s \cdot C) \quad (13)$$

where s is time scale and $G^{(s)}$ is the cumulative traffic at scale s , computed by

$$G^{(s)} = \sum_{j=0}^{s-1} G(t+j) \quad (14)$$

We intend to determine the buffer overflow probability (i.e., $P(Q_t > K)$) for cases where buffer capacity is limited, and its overflow threshold is set to K . The following is a brief introduction to the multi-scale queuing analysis proposed in [34].

In Eq. (13), time scale s is continuous. However, using discrete wavelet transform, we can only find the second-order time scale, i.e., $s = 2^j$, $j = 0, 1, \dots, n$. Thus (13) can be changed to

$$Q_D = \sup_{j \in [0, \dots, n]} (G^{(2^j)} - C \cdot 2^j) \quad (15)$$

in which $G^{(2^j)}(k) = \int_{k2^j}^{(k+1)2^j} G(t)dt$. Let $E_i = \{Q_{2^i} < K + C \cdot 2^i\}$, then

$$\mathbb{P}(Q_D > K) = 1 - \mathbb{P}(Q_D < K) = 1 - \mathbb{P}(\cap_{i=0}^n E_i) \quad (16)$$

In order to solve $\mathbb{P}(\cap_{i=0}^n E_i)$, Lemma 2 is introduced according to [34].

Lemma 2 If $E_i = \{S_i < K_i\}$, in which $S_i = X_0 + \dots + X_{i-1}$, $1 \leq i \leq n$, and X_0, \dots, X_n are independent of each other, then

$$\mathbb{P}(E_i | E_{i-1}, \dots, E_0) \geq \mathbb{P}(E_j), 1 \leq i \leq n \quad (17)$$

Accordingly, the following can be derived:

$$\begin{aligned}\mathbb{P}(Q_D > K) &= 1 - \mathbb{P}(Q_D < K) = 1 - \mathbb{P}(\cap_{i=0}^n E_i) \\ &= 1 - \mathbb{P}(E_0) \prod_{i=1}^n \mathbb{P}(E_i | E_{i-1}, \dots, E_0) \leq 1 - \prod_{i=0}^n \mathbb{P}(E_i)\end{aligned}\quad (18)$$

From Eqs. (13) and (15), it can be derived that $Q_D \leq Q_t$, it can also be expressed as $\mathbb{P}(Q_D > K) \leq \mathbb{P}(Q_t > K)$, and can further be approximated as

$$\mathbb{P}(Q_t > K) \approx 1 - \prod_{i=0}^n \mathbb{P}(E_i) \quad (19)$$

The key to multi-scale queuing analysis is to find $\mathbb{P}(E_i)$ on each time scale, i.e., $\mathbb{P}\{Q_{2^i} < K + C \cdot 2^i\}$.

5.2 Multi-scale Queuing Model

The relationship between the scale factor and the wavelet coefficients is given by Haar wavelet transform, as follows:

$$\begin{cases} U_{j,2k} = 2^{-1/2} \cdot (U_{j-1,k} + W_{j-1,k}) \\ U_{j,2k+1} = 2^{-1/2} \cdot (U_{j-1,k} - W_{j-1,k}) \end{cases} \quad (20)$$

At level j , the time scale s is set to 2^{n-j} . The cumulative traffic, denoted by $G_j(\cdot)$, its relationship with wavelet scaling coefficient is expressed as

$$G_j(k) = 2^{-j/2} \cdot U_{j,k} \quad (21)$$

Therefore, for the WGM, let

$$X_i = \begin{cases} U_{0,0}, i = 0 \\ -2^{(i-1)/2} \cdot W_{i-1,2^{i-1}-1}, \text{ otherwise} \end{cases} \quad (22)$$

then combining Eq. (21) and (22), it can be inferred that

$$G_j = 2^{-j} \cdot \sum_{i=0}^j X_i = 2^{-j} \cdot S_j \quad (23)$$

Let

$$K_j = K \cdot 2^j + C \cdot 2^n \quad (24)$$

then

$$E_i = \{G_i < K + C \cdot 2^i\} = \{S_i < K_i\} \quad (25)$$

This satisfies the condition of Lemma 2. Therefore, for the queuing analysis based on the WGM, we summarize the following theorem:

Theorem 1 Assuming that the parameters of scaling coefficient GAR model are α , λ , and the j -th wavelet coefficients are μ_j and σ_j , then for the WGM, the buffer overflow probability can be calculated using Eq. (19), and

$$\begin{aligned}\mathbb{P}(E_i) &= \mathbb{P}(S_i < K_i) \\ &= \begin{cases} \text{Gam}(K_i), \text{if } i = 0 \\ \frac{\lambda^\alpha}{\Gamma(\alpha) \cdot \sqrt{2\pi\sigma}} \cdot \int_{-\infty}^{K_i} e^{-\frac{(x-\mu)^2}{2\sigma^2}} dx \cdot \int_0^{K_i-x} y^{\alpha-1} \cdot e^{-\lambda y} dy, \text{otherwise} \end{cases} \quad (26)\end{aligned}$$

where $\text{Gam}(\cdot)$ is the probability distribution function of the Gamma distribution, i.e.,

$$\text{Gam}(K_i) = \int_0^{K_i} \frac{\lambda^\alpha \cdot x^{\alpha-1} \cdot e^{-\lambda x}}{\Gamma(\alpha)} dx, \quad \Gamma(\alpha) = \int_0^\infty t^{\alpha-1} \cdot e^{-t} dt \quad (27)$$

μ and σ are computed by

$$\begin{cases} \mu = -\sum_{j=0}^{i-1} 2^{j/2} \cdot \mu_j \\ \sigma = \sqrt{\sum_{j=0}^{i-1} 2^j \cdot \sigma_j^2} \end{cases} \quad (28)$$

Proof For Eq. (26), there are two cases to discuss:

1. When $i = 0$, we have $S_0 = U_{0,0}$, and $\mathbb{P}(E_0) = \text{Gam}(K_0)$.
2. For the case where $i > 0$, we have

$$S_i = U_{0,0} + W_{S_i} = U_{0,0} - \sum_{j=1}^i 2^{(i-j)/2} \cdot W_{j-1,2^{j-1}-1} \quad (29)$$

Equation (29) consists of $U_{0,0}$ and W_{S_i} . The former satisfies Gamma distribution, and the latter represents the sum of several independent Gaussian distributions (which have been proved) and still follows Gaussian distribution. Let $\mathbb{E}(W_{S_i}) = \mu$ and $\mathbb{D}(W_{S_i}) = \sigma^2$, then based on the property of Gaussian distribution we have (28). Thus, S_i can be seen as the sum of a random variable subject to Gamma distribution and a random variable of a Gaussian distribution whose probability distribution is a joint distribution of two random variables. From the knowledge of probability theory and mathematical analysis, it can be deduced that

$$\begin{aligned}
\mathbb{P}(E_i) &= \mathbb{P}(S_i < K_i) \\
&= \frac{1}{\sqrt{2\pi}\sigma} e^{-\frac{(x-\mu)^2}{2\sigma^2}} \times \frac{\lambda^\alpha}{\Gamma(\alpha)} \cdot y^{\alpha-1} \cdot e^{-\lambda \cdot y} dx dy \\
&= \int_{-\infty}^{K_i} \frac{1}{\sqrt{2\pi}\sigma} \cdot e^{-\frac{(x-\mu)^2}{2\sigma^2}} dx \int_0^{K_i-x} \frac{\lambda^\alpha}{\Gamma(\alpha)} \cdot y^{\alpha-1} \cdot e^{-\lambda \cdot y} dy \\
&= \frac{\lambda^\alpha}{\Gamma(\alpha) \cdot \sqrt{2\pi} \cdot \sigma} \int_{-\infty}^{K_i} e^{-\frac{(x-\mu)^2}{2\sigma^2}} dx \int_0^{K_i-x} y^{\alpha-1} \cdot e^{-\lambda \cdot y} dy
\end{aligned} \tag{30}$$

In Eq. (30), we can see that both Gaussian distribution and the original function of Gamma distribution cannot be represented by elementary functions. For example, the following integral solution can be obtained by calculation:

$$\begin{aligned}
&\int_0^{K_i-x} y^{\alpha-1} \cdot e^{-\lambda \cdot y} dy \\
&= \frac{e^{-\lambda \cdot (K_i-x)/2}}{\alpha \cdot \lambda^\alpha} \cdot \left[\frac{1}{1+\alpha} \cdot (\lambda \cdot (K_i-x))^{\frac{\alpha}{2}} \cdot \text{WhittakerM}\left(\frac{\alpha}{2}, \frac{(\alpha+1)}{2}, \lambda \cdot (K_i-x)\right) \right. \\
&\quad \left. + (\lambda \cdot (K_i-x))^{\frac{\alpha}{2}-1} \cdot \text{WhittakerM}\left(\frac{\alpha}{2} - 1, \frac{(\alpha+1)}{2}, \lambda \cdot (K_i-x)\right) \right]
\end{aligned} \tag{31}$$

where $\text{WhittakerM}(\cdot)$ is the solution to the hypergeometric Whittaker function. In our model, α and λ can be estimated using the specific value, K_i , which also has a specific value in the calculation. The probability $\mathbb{P}(E_i)$ can be calculated in this way, and the overflow probability can be further calculated according to Eq. (19). \square

5.3 Storage Model

In this section, a storage model for network buffer is built, based on which the theoretical value of delay and delay jitter of a video stream is derived.

Let Q_t represent the queue length of the buffer at time t , and $\varepsilon = P(Q_t > K)$ denote the buffer overflow probability. The storage probability for Q_t can be expressed by $1 - \varepsilon$. According to the theoretical basis provided by Sect. 5.1, the Q_t can be expressed as the queue length of buffer on each time scale under the framework of multi-scale discrete wavelet transform. Thus, the storage probability can be computed by

$$1 - \varepsilon = 1 - \mathbb{P}(Q_t > K) = \prod_{i=0}^n \mathbb{P}(E_i) \tag{32}$$

where $P(E_i)$ is as shown in Eq. (26). We know that if node buffer is limited and the rule of the self-similar queuing system is FIFO, the waiting time for a newly arrived video traffic must be the time required for all the tasks in the current queuing system to be completed, which is computed by

$$T_d = \frac{Q_t}{C} \quad (33)$$

According to probability distribution function of Q_t obtained by Eq. (3), we can get the mean and variance of T_d , representing delay and delay jitter, i.e.,

$$\begin{aligned} E[T_d] &= E\left[\frac{Q_t}{C}\right] = \frac{1}{C} \cdot E[Q_t] \\ &= \frac{1}{C} \cdot \sum_{i=0}^n Q_i (1 - P(Q_t > K)) \\ &= \frac{1}{C} \cdot \sum_{i=0}^n Q_i \cdot \left(\prod_{j=0}^i P(E_j) \right) \end{aligned} \quad (34)$$

and

$$\mathbb{D}[T_d] = \mathbb{E}[T_d^2] - (\mathbb{E}[T_d])^2 = \frac{[\mathbb{E}(Q_t^2) - \mathbb{E}(Q_t)^2]}{C^2} \quad (35)$$

Substituting Q_i in (15) into (34) and (35), the delay and delay jitter of wireless video streaming can be obtained.

6 Simulation Analysis of the WGM Queuing System

In previous sections, the queuing model for the wireless video stream and its theoretical calculation for buffer overflow probability, delay, and delay jitter are given. Next, we conduct a simulation queuing analysis. The buffer overflow probability is first simulated and

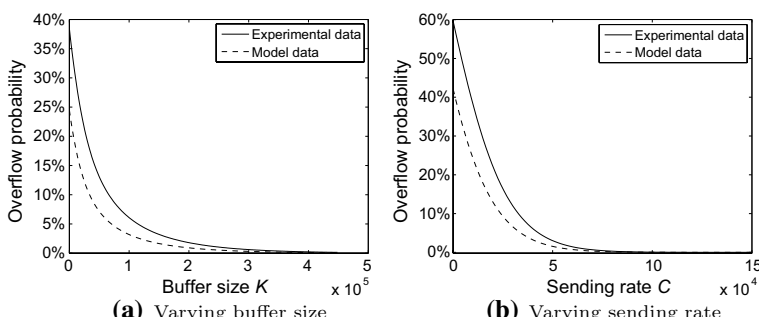


Fig. 6 Comparison between experimental data and model data

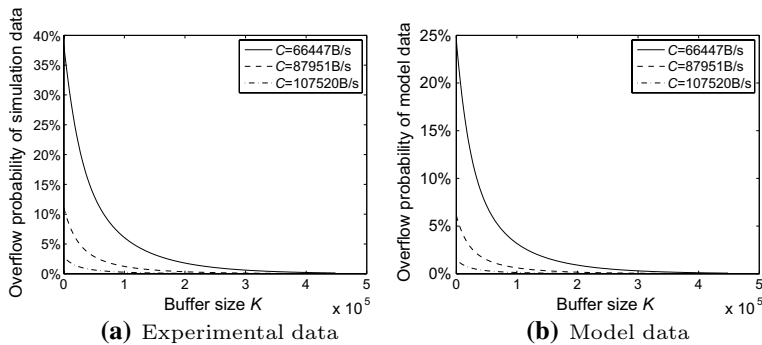


Fig. 7 Buffer overflow probability as a function of buffer size

analyzed in detail. Then, the delay and delay jitter are simulated and analyzed carefully. In our study, experimental results are obtained by using Matlab.

6.1 Simulation Results: Buffer Overflow Probability

We design four simulation experiments in this section, focusing largely on the sensitivity of buffer overflow probability to buffer size and sending rate.

6.1.1 Overview

The first simulation experiment illustrates the general effects of buffer size K on the overflow probability of video streaming when C is set to 66,447 B/s. These impacts can be observed in Fig. 6a. The probability of buffer overflow gradually decreases with the increase of K and approximately showing the trend of hyperbolic attenuation. The difference between experimental data and model data is to some extent caused by the randomness of data generated by the mathematical model. The small errors of α and λ from estimation in scaling coefficient model are reflected. The second experiment mainly investigates the trend of buffer overflow probability with the change of C when K is fixed to 265,800 B. As shown in Fig. 6b, the probability of buffer overflow dramatically decreases with the increase of sending rate, showing an approximately exponential decay.

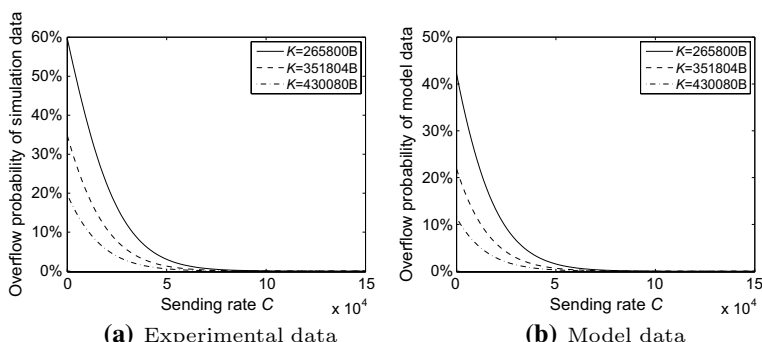


Fig. 8 Buffer overflow probability as a function of sending rate

It can be concluded that the impact of sending rate on buffer overflow probability is higher than that of buffer size. Increasing the sending rate of buffer data has a better effect of reducing the overflow probability.

6.1.2 Impact of Buffer Sizes

The purpose of the third experiment is to see the change of overflow probability of experimental data and model data with respect to buffer size K is obtained by analyzing C at 66,447 B/s, 87,951 B/s, and 107,520 B/s, respectively. From Fig. 7, we can see that no matter what kind of data is analyzed, when C is set to 107,520 B/s, the value of overflow probability is minimal, and the magnitude of the change is relatively small and stable with the increase of buffer. Regardless of the value of C , the overflow probability shows hyperbolic attenuation with an increase of K . Second, when C takes a different value, the value of K that makes overflow probability close to zero also changes dramatically. Also, the range of overflow probability of model data is less than that of experimental data.

6.1.3 Impact of Sending Rate

The next experiment studies the changes in overflow probability of experimental data and model data concerning C when K is set at 26,5800 B, 35,1804 B, and 430,080 B, respectively. It can be seen from Fig. 8 that when the buffer threshold K is relatively large, a smaller C can reduce the overflow probability effectively; regardless of the value of K , the overflow probability still shows exponential decay; when K takes different values, the value of C (that makes the overflow probability become 0) is almost unchanged. This tendency indicates that although the increase of network buffer can reduce overflow, the determinant factor that reduces or eliminates the overflow probability is C . There is a similar phenomenon in Fig. 7 that the range of overflow probability of model data becomes small.

6.1.4 Summary of Results

The overflow probability of model data in these experiments all shows a decreasing trend, mainly because model data are more regular than experimental data. It is no longer as messy as the simulated data. This regularity changes the values of α and λ in the Gamma model of the scale factor. The change, though not significant, can be observed. In the

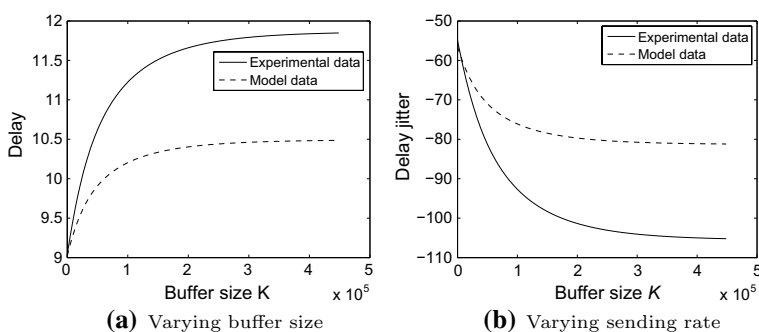


Fig. 9 Comparison between experimental data and model data with varying buffer size

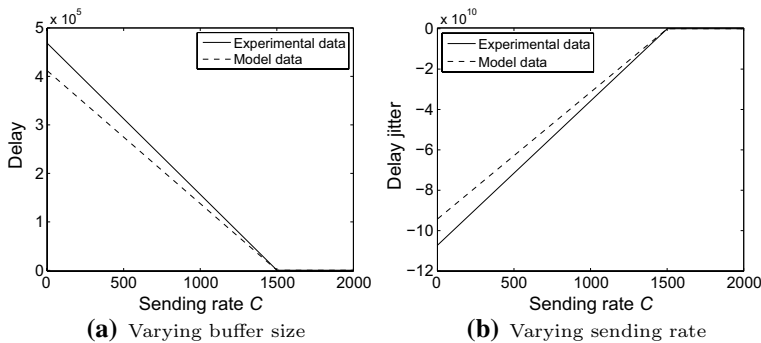


Fig. 10 Comparison between experimental data and model data with varying sending rate

subsequent analysis of the delay and delay jitter simulation, this phenomenon can appear many times and will not be repeated.

6.2 Simulation Results: Delay and Delay Jitter

The analysis of delay and delay jitter of wireless video traffic is also divided into four experiments. With wavelet analysis, each level of data series is only expressed in terms of time scales, in which the durations are not specifically given in seconds. Therefore, the follow-up analysis focuses on qualitative analysis to provide reference and directional guidance for the prediction of video communication performance. With (34) and (35), it can be inferred that the delay and delay jitter are infinite when C is set to 0. Thus, we replace $C = 0$ with $C = 1$ in the calculation.

6.2.1 Overview

The first experiment examines the variation of delay and delay jitter for K , where C is fixed to 66,447 B/s. These variations are shown in Fig. 9. From Fig. 9a, the delay is not reduced with network buffer, but first increases and then gradually stabilizes. Turning to Fig. 9b, the y-axis shows a negative jitter, which does not affect our evaluation

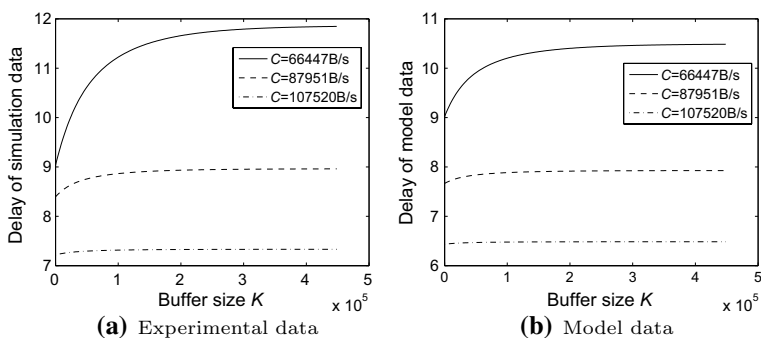


Fig. 11 Delay as a function of buffer size

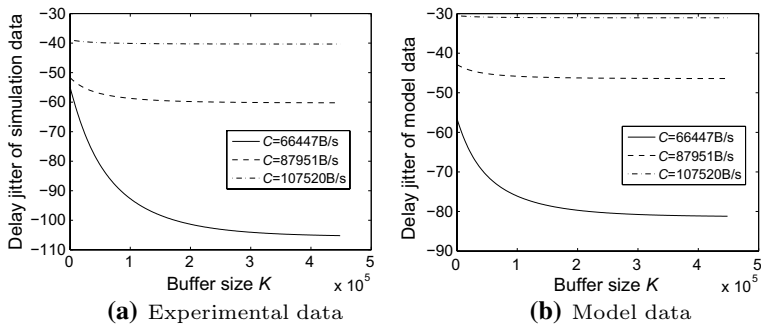


Fig. 12 Delay jitter as a function of buffer size

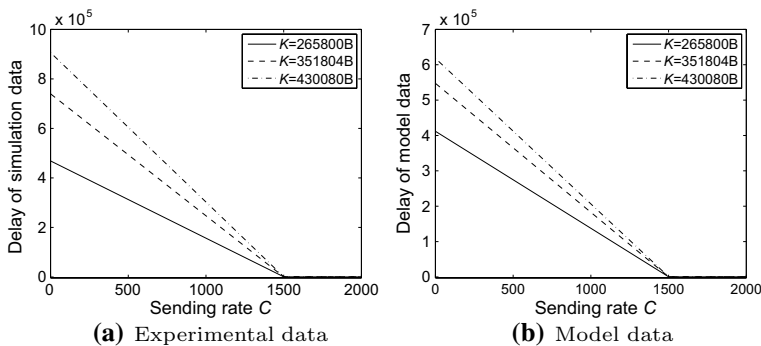


Fig. 13 Delay as a function of sending rate

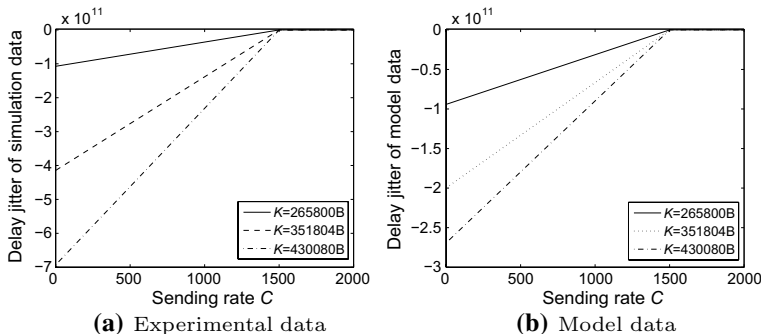


Fig. 14 Delay jitter as a function of sending rate

for this change. If the absolute value of jitter is used for evaluation and sending rate is fixed, the delay jitter increases first with the increase of K and then stabilizes.

The results of the second experiment are to look at the variation of delay and delay jitter with respect to C when $K = 265,800$ B. It can be seen from Fig. 10a that with an increase of C , the delay reduces rapidly. Because C has enormous jumps, only two curves that are almost coincident with the y - and x -axis are seen if the x -axis shows all the values of C . For

this reason, only part of the points is shown here. The attenuation of delay is approximately a straight line as C increases, but in fact, the delay shows approximately exponential decay. Figure 10b reveals the trend of delay jitter change when K is fixed to 265,800 B. Because the y-axis is negative, we use its absolute value for evaluation. With the increase of C , the jitter becomes smaller. Similarly, model data shows a smaller jitter range than experimental data. The fourth experiment also shows the same phenomenon.

6.2.2 Impact of Buffer Sizes

The purpose of the third experiment is to explore the variation of the delay and delay jitter with K when C is 66,447 B/s, 87,951 B/s and 107,520 B/s, respectively. It can be seen from Fig. 11 that when C is relatively large, the delay of wireless streaming media is almost stable; when C is relatively small, the buffer has a more significant impact on the delay, which first increases with the buffer and then becomes stable. Besides, the range of model data delay is smaller than that of experimental data. From Fig. 12, the absolute value of delay jitter is also used for evaluation, which shows a similar trend as in Fig. 11.

6.2.3 Impact of Sending Rate

The results of the fourth experiment reveal the variation of delay and delay jitter with C when K is 265,800 B, 351,804 B, and 430,080 B. It is clear that with the increase of C , the delay is drastically reduced in Fig. 13. Similarly, the model data has a smaller range of delay than experimental data. In addition, there is an interesting phenomenon: when C is small and has not reached a certain value, the higher the buffer, the greater the delay. In Fig. 14, which mainly studies the variation of jitter with the transmission rate when K is different. We can see that it has the same trend as shown in Fig. 13.

6.2.4 Summary of Results

The purpose of the third experiment is to see the change of overflow probability of experimental data and model data concerning buffer size K is obtained by analyzing C at 66,447 B/s, 87,951 B/s, and 107,520 B/s, respectively. Form Fig. 7, we can see that no matter what kind of data is analyzed, when C is fixed to 107,520 B/s, the value of overflow probability is minimal, and the magnitude of the change is relatively small and stable with the increase of buffer. Regardless of the value of C , the overflow probability shows hyperbolic attenuation with the increase of K . Second, when C takes a different value, the value of K that makes overflow probability close to zero also changes dramatically. Also, the range of overflow probability of model data is less than that of experimental data.

7 Summary and Conclusions

This paper presents a Wavelet-based Gamma Model (WGM) to model multi-hop video traffic based on the characteristic analysis of typical wireless video traffic. First, two wireless video streams through simulation are generated, which correspond to *static multi-hop network* and *dynamic multi-hop network*. They have all the characteristics of network traffic, including self-similarity. Second, the WGM generates two types of experimental data. The results demonstrate that the model data also shows all the characteristics of network traffic. By analyzing the fitting degree of autocorrelation, PDF, and CDF of experimental data and model data, we find that the WGM can reflect the various characteristics of multimedia traffic in wireless multi-hop networks. By observing the self-similarity of experimental data and model data, we confirm the accuracy of our model. Lastly, we deduce the theoretical value of overflow probability, delay, and delay jitter based on the WGM and verify the accuracy by experimental data.

Our results show that the overflow probability decays hyperbolically and exponentially with the increase in network buffer and transmission rate. We also find that the delay and delay jitter of wireless video streaming first increase and then stabilize with the increase in buffer size, and delay and delay jitter decrease sharply with the increase of sending rate. This study is helpful for the performance improvement of wireless video service.

Acknowledgements This work was supported in part by the National Natural Science Foundation of China under Grant Nos. 61502230 and 61073197, in part by the Natural Science Foundation of Jiangsu Province under Grant No. BK20150960, in part by the National Key R&D Program of China under Grant No. 2018YFC0808500, in part by the Natural Science Foundation of the Jiangsu Higher Education Institutions of China under Grant No. 15KJB520015, in part by the National Engineering Research Center Program of Communications and Networking under Grant No. GCZX012, in part by the Nanjing Municipal Science and Technology Plan Project under Grant No. 201608009. The first author is especially grateful to the Jiangsu Government Scholarship for Overseas Studies assisting his research abroad.

References

1. Ericsson, A. B. (2017). *Ericsson mobility report: On the pulse of the networked society*. Ericsson, Sweden, Tech. Rep. EAB-17.
2. Fontugne, R., Abry, P., Fukuda, K., Veitch, D., Cho, K., Borgnat, P., et al. (2017). Scaling in internet traffic: A 14 year and 3 day longitudinal study, with multiscale analyses and random projections. *IEEE/ACM Transactions on Networking*, 25(4), 2152–2165.
3. Chaurasia, A., & Sehgal, V. K. (2015). Optimal buffer-size by synthetic self-similar traces for different traffics for NoC. *SIGBED Review*, 12(3), 6–12.
4. Min, G., & Jin, X. (2013). Analytical modelling and optimization of congestion control for prioritized multi-class self-similar traffic. *IEEE Transactions on Communications*, 61(1), 257–265.
5. Lin, S.-C., Wang, P., Akyildiz, I. F., & Luo, M. (2016). Throughput-optimal LIFO policy for bounded delay in the presence of heavy-tailed traffic. In *Proceedings of IEEE GLOBECOM* (pp. 1–7).
6. Wang, P., & Akyildiz, I. F. (2015). On the stability of dynamic spectrum access networks in the presence of heavy tails. *IEEE Transactions on Wireless Communications*, 14(2), 870–881.
7. Kalbkhani, H., Shayesteh, M. G., & Haghighat, N. (2017). Adaptive Istar model for long-range variable bit rate video traffic prediction. *IEEE Transactions on Multimedia*, 19(5), 999–1014.
8. Kastrinakis, M., Badawy, G., Smadi, M. N., & Koutsakis, P. (2017). Video frame size modeling for user-generated traffic in an enterprise-like environment. *Computer Communications*, 109(5), 24–37.
9. Toral-Cruz, H., Pathan, A.-S. K., & Pacheco, J. C. R. (2013). Accurate modeling of voip traffic qos parameters in current and future networks with multifractal and Markov models. *Mathematical and Computer Modelling*, 57(11), 2832–2845.
10. Jin, X., & Min, G. (2007). Performance modelling of priority queuing discipline under self-similar and poisson traffic. In *Proceedings of IEEE LCN* (pp. 567–574).

11. Adas, A. (1997). Traffic models in broadband networks. *IEEE Communications Magazine*, 35(7), 82–89.
12. Willinger, W., Taqqu, M. S., Sherman, R., & Wilson, D. V. (1997). Self-similarity through high-variability: Statistical analysis of ethernet lan traffic at the source level. *IEEE/ACM Transactions on Networking*, 5(1), 71–86.
13. Yang, X., & Petropulu, A. P. (2001). The extended alternating fractal renewal process for modeling traffic in high-speed communication networks. *IEEE Transactions on Signal Processing*, 49(7), 1349–1363.
14. Mandelbrot, B. B., & Van Ness, J. W. (1968). Fractional brownian motions, fractional noises and applications. *SIAM Review*, 10(4), 422–437.
15. Hosking, J. R. M. (1981). Fractional differencing. *Biometrika*, 68(1), 165–176.
16. Girma, D., Lazaro, O., & Dunlop, J. (2000). Online video traffic modelling with wavelet transform. *Electronics Letters*, 36(16), 1368–1370.
17. Wang, P., & Akyildiz, I. F. (2011). Spatial correlation and mobility-aware traffic modeling for wireless sensor networks. *IEEE/ACM Transactions on Networking*, 19(6), 1860–1873.
18. Jin, X., & Min, G. (2009). Modelling and analysis of priority queueing systems with multi-class self-similar network traffic: A novel and efficient queue-decomposition approach. *IEEE Transactions on Communications*, 57(5), 1444–1452.
19. Ghosh, A., Jana, R., Ramaswami, V., Rowland, J., & Shankaranarayanan, N. K. (2011). Modeling and characterization of large-scale wi-fi traffic in public hot-spots. In *Proceedings of IEEE INFOCOM* (pp. 2921–2929).
20. Ma, S., & Ji, C. (1998). Modeling video traffic in the wavelet domain. In *Proceedings of IEEE INFOCOM* (pp. 201–208).
21. Leland, W. E., Taqqu, M. S., Willinger, W., & Wilson, D. V. (1994). On the self-similar nature of ethernet traffic (extended version). *IEEE/ACM Transactions on Networking*, 2(1), 1–15.
22. Crovella, M. E., & Bestavros, A. (1997). Self-similarity in world wide web traffic: Evidence and possible causes. *IEEE/ACM Transactions on Networking*, 5(6), 835–846.
23. Bai, G., & Williamson, C. (2004). Time-domain analysis of web cache filter effects. *Performance Evaluation*, 58(2), 285–317.
24. Sahinoglu, Z., & Tekinay, S. (1999). On multimedia networks: Self-similar traffic and network performance. *IEEE Communications Magazine*, 37(1), 48–52.
25. Karagiannis, T., Molle, M., Faloutsos, M., & Broido, A. (2004). A nonstationary Poisson view of internet traffic. In *Proceedings of INFOCOM* (pp. 1558–1569).
26. Borgnat, P., Dewaele, G., Fukuda, K., Abry, P., & Cho, K. (2009). Seven years and one day: Sketching the evolution of internet traffic. In *Proceedings of INFOCOM* (pp. 711–719).
27. Yin, S., & Lin, X. (2005). Traffic self-similarity in mobile ad hoc networks. In *Proceedings of IFIP WOCN* (pp. 285–289).
28. Tickoo, O., & Sikdar, B. (2003). On the impact of IEEE 802.11 mac on traffic characteristics. *IEEE Journal on Selected Areas in Communications*, 21(2), 189–203.
29. Oliveira, C., Kim, J. B., & Suda, T. (2003). Long-range dependence in IEEE 802.11 b wireless LAN traffic: An empirical study. In *Proceedings of IEEE CCW* (pp. 17–23).
30. Jie, Y., & Petropulu, A. P. (2006). Study of the effect of the wireless gateway on incoming self-similar traffic. *IEEE Transactions on Signal Processing*, 54(10), 3741–3758.
31. Ge, X., Yang, Y., Wang, C.-X., Liu, Y.-Z., Liu, C., & Xiang, L. (2010). Characteristics analysis and modeling of frame traffic in 802.11 wireless networks. *Wireless Communications and Mobile Computing*, 10(4), 584–592.
32. Li, X., Lu, H., & Lu, H. (2013). QoS analysis of self-similar multimedia traffic with variable packet size in wireless networks. In *Proceedings of VTC Fall* (pp. 1–5).
33. Tewfik, A. H., & Kim, M. (1992). Correlation structure of the discrete wavelet coefficients of fractional brownian motion. *IEEE Transactions on Information Theory*, 38(2), 904–909.
34. Ribeiro, V. J., Riedi, R. H., Crouse, M. S., & Baraniuk, R. G. (2000). Multiscale queuing analysis of long-range-dependent network traffic. In *Proceedings of IEEE INFOCOM* (pp. 1026–1035).

Publisher's Note Springer Nature remains neutral with regard to jurisdictional claims in published maps and institutional affiliations.



Hang Shen received the Ph.D. degree in computer science from the Nanjing University of Science and Technology, Nanjing, China. Since 2015, he has been an Assistant Professor with the Department of Computer Science and Technology, Nanjing Tech University, Nanjing, China. His research interests include traffic modeling and analysis for multimedia networks, and network slicing and security for 5G networks. He is a member of the IEEE and a member of the ACM.



Guangwei Bai received the B.Eng. (1983) and M.Eng. (1986) from the Xi'an Jiaotong University, China, both in computer engineering. He received the Ph.D. in Computer Science (1999) from the University of Hamburg, Germany. From 1999 to 2001, he worked at the German National Research Center for Information Technology, Germany, as a Research Scientist. In 2001, he joined the University of Calgary, Canada, as a Research Associate. Since 2005, he has been working at the Nanjing Tech University in China, as a Professor in Computer Science. In 2011, he was a Visiting Professor with the University of Waterloo in Canada. His research interests are in 5G mobile technology, multimedia QoS/QoE, network security, and privacy protection. He is a member of the ACM.



Junyuan Wang received a B.Sc. in Mathematics and an M.Sc. in Computer Science both from Nanjing Tech University, and is now an Engineer at Huawei Technologies. His research interests include traffic model and multimedia communications.



Lu Zhao received a B.Sc. (2007) in Mathematics from School of Science, Nanjing University of Aeronautics and Astronautics in China, an M.Sc. (2010) in Computer Science from the College of Computer Science and Technology, Nanjing Tech University in China, and is now a Ph.D. student in the College of Computer Science and Engineering, Nanjing University of Science and Technology, China. Her research interests include wireless multimedia sensor networks, multimedia communications, and traffic model.